Synthesis and Structures of Neutral Crystals and Charge-Transfer Salts of Selenium Containing TMET-TTP Derivatives

Minoru Ashizawa, Hirofumi Nii, Takehiko Mori,* Yohji Misaki,† Kazuyoshi Tanaka,† Kazuo Takimiya,†† and Tetsuo Otsubo††

Department of Organic and Polymeric Materials, Graduate School of Science and Engineering, Tokyo Institute of Technology, O-okayama, Meguro-ku, Tokyo 152-8552

†Department of Molecular Engineering, Graduate School of Engineering, Kyoto University, Yoshida, Kyoto 606-8501

††Department of Applied Chemistry, Graduate School of Engineering, Hiroshima University, Higashi-Hiroshima 739-8527

Received March 4, 2003; E-mail: takehiko@o.cc.titech.ac.jp

TMET-TTP derivatives in which one or both of the outer 1,3-dithiole rings are replaced by 1,3-diselenole rings (**1a**–**1d**) have been prepared (TMET-TTP: 2-[4,5-bis(methylthio)-1,3-dithiol-2-ylidene]-5-(4,5-ethylenedithio-1,3-dithiol-2-ylidene)-1,3,4,6-tetrathiapentalene). The neutral crystal of **1c** has β-type uniform stacks, whereas **1a** shows a θ-type molecular arrangement in the neutral crystal. The AsF_6 salts of **1a** and **1d** have a θ-type structure similarly to other TMET-TTP salts. In spite of the relatively small dihedral angle (117°), the conductivity is weakly semiconductive from room temperature. Selenium substitution causes unbalance of the diagonal intermolecular interactions, which may be the origin of a deviation from the universal phase diagram of the θ-phase.

Bis-fused TTF derivatives (TTP: tetrathiapentalene) are excellent organic donors, which form highly conducting radical-cation salts with a variety of anions.[1] Since these donors construct a two-dimensional network for electrical conduction, many of the radical-cation salts are stable metals down to low temperatures. Among them, TMET-TTP (Scheme 1) has a strong tendency to form a θ-phase arrangement regardless of the counter anions.[2] The conducting properties of the θ-phase salts change systematically from an insulator to a metal as a function of the dihedral angle between the molecular planes.[3] The dihedral angles of the θ-phase TMET-TTP salts are around 128°, which fall into the insulating region. Actually, these salts exhibit almost constant conductivity down to 200 K, and become semiconducting below this temperature. On the other hand, the AsF_6 salt is exceptional; the salt shows a metallic behavior down to liquid-helium temperatures. Although the structure of the AsF_6 salt has not been solved, the lattice constants are the same as those of the θ-phase TMET-TTP salts, indicating an isostructural arrangement to the θ-phase.[4]

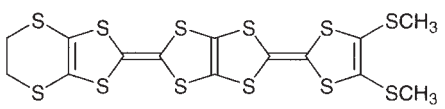

TMET-TTP

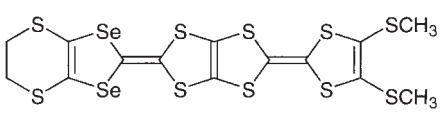

TMET-TS-TTP

Scheme 1. TMET-TTP type organic donors.

In order to improve the conducting properties, we have attempted to introduce selenium atoms into the TMET-TTP molecule. Along this line, we have reported TMET-TS-TTP (Scheme 1), where the two sulfur atoms of the terminal 1,3-dithiole rings are replaced by selenium atoms.[5] Except for $(TMET\text{-}TS\text{-}TTP)_2(TCNQ)$, which shows metallic conductivity down to 120 K, many of the charge-transfer salts are semiconductive. In the present work, we report more systematic synthesis of the selenium containing TMET-TTP derivatives, **1a**–**1d**, as well as the structures of the neutral crystals and the AsF_6 salts.

Results and Discussion

Synthesis. The synthesis of selenium analogues of TMET-TTP is outlined in Scheme 2. In order to introduce selenium, we used 1,3-diselenole-2-selone prepared from carbon diselenide as the key starting material.[6] 4,5-Bis(methylseleno)-1,3-diselenole-2-selone, 4,5-bis(methylthio)-1,3-diselenole-2-selone, and 4,5-ethylenediseleno-1,3-diselenole-2-selone were prepared via lithiation to this compound,[7] and converted to the corresponding ketones **3** and **8** by using $Hg(OAc)_2$. The construction of the TTP framework was accomplished by two-step phosphite-mediated coupling reactions via deprotection of the cyanoethyl groups. In these coupling reactions, we adopted combinations of 1,3-diselenol-2-one and 1,3-dithiole-2-thione. This led to relatively high yields compared to other combinations; the direct phosphite-mediated coupling of 1,3-diselenole-2-selone with 1,3-dithiole-2-thione or ketone did not proceed smoothly, and resulted in low yields.

Electrochemistry. The solution redox properties of newly prepared TMET-TTP derivatives have been studied by cyclic

Published on the web November 15, 2003; DOI 10.1246/bcsj.76.2091

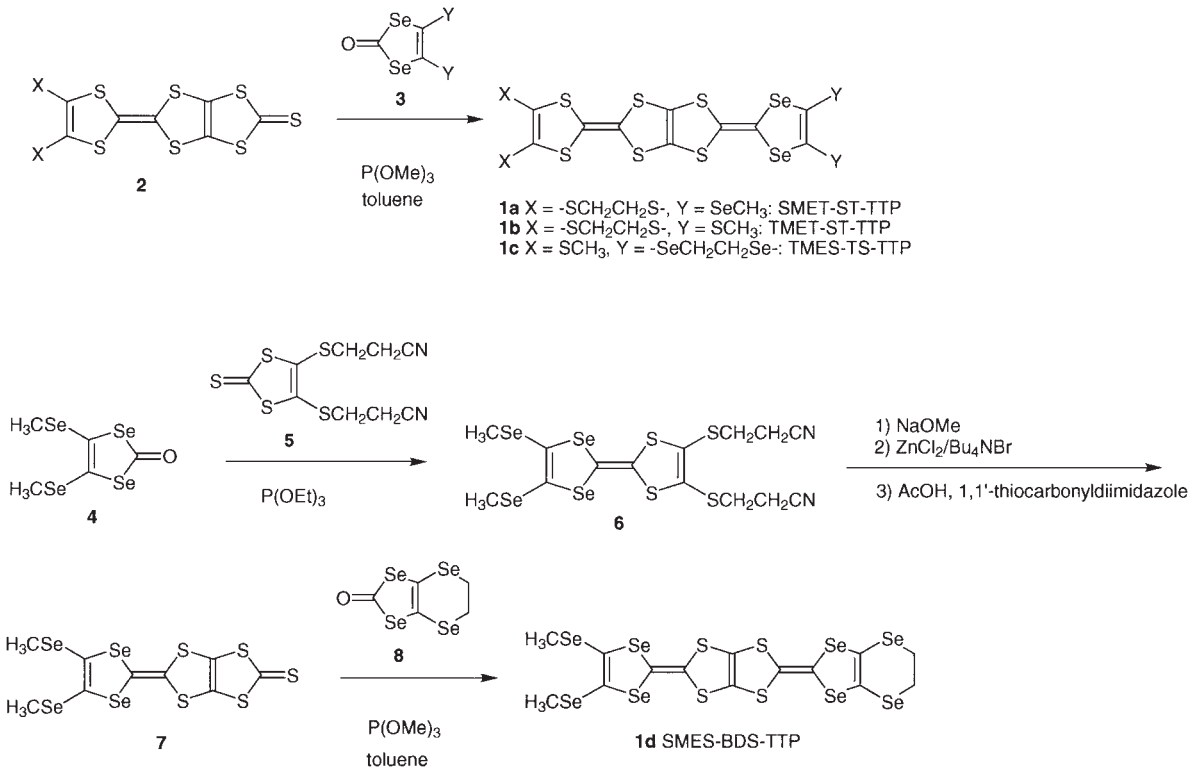

Scheme 2. Synthesis of selenium substituted TMET-TTP derivatives.

Table 1. Redox Potentials/V[a)]

Compound	$E^1_{1/2}$	$E^2_{1/2}$	$E^3_{1/2}$	E^4_{ox}	$E_2 - E_1$
1a	0.45	0.69	0.91	1.12[b)]	0.24
1b	0.42	0.65	0.90	1.18[b)]	0.23
1c	0.46	0.70	0.92	1.16[b)]	0.24
1d	0.48	0.73	0.95	1.17[b)]	0.25
TMET-TTP	0.44	0.68	0.90	1.05	0.24

a) vs Ag/AgCl in *n*-Bu_4NPF_6/Benzonitrile at a Pt working electrode, 25 °C, scan rate 25, 50, and 100 mV s^{-1}. The listed values are averages for the three scan rates. As a reference, the redox potential of ferrocene is 0.46 V under identical conditions. b) The oxidation peaks are shown on account of the irreversibility, except for $E^4_{1/2}$ for TMET-TTP.

voltammetry (Table 1). These donors show four redox waves up to tetra cations in accordance with the existence of the four 1,3-dithiole and 1,3-diselenole rings. In general, Se substitution of the terminal groups (–SCH_3 → –$SeCH_3$) improves the donor ability, whereas Se substitution of the 1,3-dithiole rings (TTF → TSF) weakens it. The first redox potential of SMES-BDS-TTP (**1d**), where both terminal groups and the 1,3-dithiole rings are replaced by selenium atoms, is 0.04 V higher than that of TMET-TTP. This demonstrates that the effect of ring substitution is stronger than the influence of terminal substitution.

Neutral crystals of SMET-ST-TTP (**1a**) and TMES-TS-TTP (**1c**) were obtained as red and orange rods by slow evaporation of carbon disulfide–hexane solutions. Electrochemical crystal growth of the present donors in the presence of *n*-Bu_4NAsF_6 in chlorobenzene afforded plate-like crystals of (SMET-ST-TTP: **1a**)$(AsF_6)_{0.32}$ and (SMES-BDS-TTP: **1d**)$(AsF_6)_{0.35}$. Although we attempted crystal growth with various anions, other salts were not obtained with sufficient quality for an X-ray structure analysis.

Table 2. Crystallographic Data of the Neutral Crystals

	SMET-ST-TTP (**1a**)	TMES-TS-TTP (**1c**)
Chemical formula	$C_{14}H_{10}S_8Se_4$	$C_{14}H_{10}S_4Se_8$
Formula weight	750.55	1032.61
Shape	Red needle	Red needle
Crystal system	Triclinic	Orthorhombic
Space group	$P\bar{1}$	$P2_12_12_1$
a/Å	11.440(3)	7.901(3)
b/Å	28.78(1)	47.86(2)
c/Å	7.471(2)	6.001(2)
α/°	94.97(2)	90
β/°	102.93(2)	90
γ/°	101.18(2)	90
V/Å^3	2331(1)	2269(1)
Z	4	4
D_{calc}/g cm^{-3}	2.139	2.197
Temperature	r.t.	r.t.
$R^{a)}/R_w^{b)}$	0.094/0.111	0.112/0.120
Reflections used	4266 ($I > 3.0\sigma(I)$)	1548 ($I > 3.0\sigma(I)$)

a) $R = \Sigma||F_o| - |F_c||/\Sigma|F_o|$. b) $R_w = [\Sigma w(|F_o| - |F_c|)^2/\Sigma w{F_o}^2]^{1/2}$.

Crystal Structure of Neutral Crystals. Single crystal X-ray structure analyses have been carried out for neutral crystals of SMET-ST-TTP (**1a**) and TMES-TS-TTP (**1c**). The crystal data are listed in Table 2. Despite the similarity of the molecules, **1a** and **1c** form entirely different types of crystals, where the space group is different: $P\bar{1}$ for SMET-ST-TTP (**1a**) and

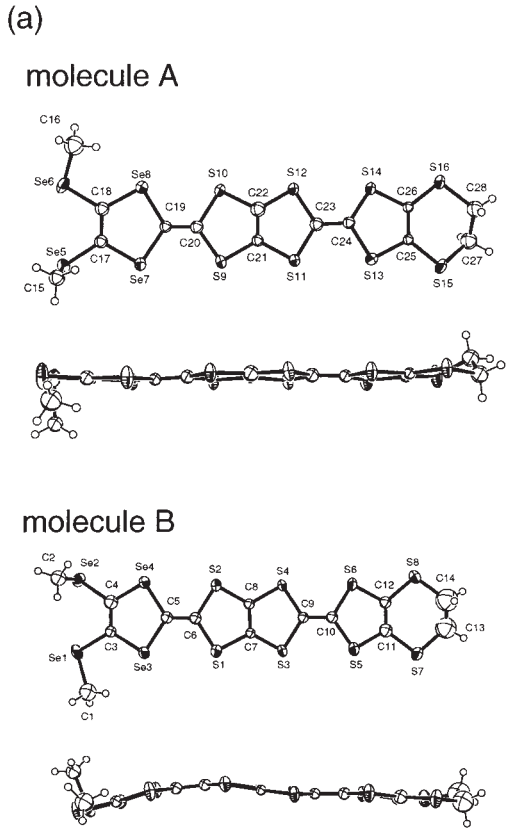

Fig. 1. ORTEP drawing and overlap mode of neutral SMET-ST-TTP (**1a**). (a) Crystallographically independent molecules A and B and (b) overlap mode of the molecule A.

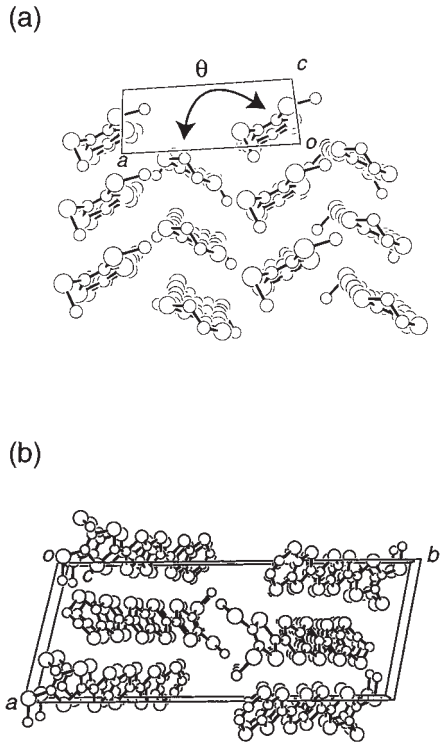

Fig. 2. Crystal structures of neutral SMET-ST-TTP (**1a**). (a) View along the molecular long axis and (b) projection on the *ab* plane.

$P2_12_12_1$ for TMES-TS-TTP (**1c**). This is the first report concerning the neutral structure of TMET-TTP derivatives.

SMET-ST-TTP (1a): The molecular structure and the overlap mode of neutral SMET-ST-TTP (**1a**) are shown in Figs. 1(a) and 1(b). Two molecules, A and B, are crystallographically independent, and form two independent columns. Molecule A is almost planar. On the other hand, molecule B has a bent shape. One of the two terminal methylthio groups extends out of the molecular plane, and the other is located in the plane. These structural features of the terminal methylthio groups resemble the molecules in charge-transfer salts (the partly in-plane methylthio group),[8] rather than the neutral crystal of TTM-TTP (standing methylthio groups) (TTM-TTP: 2,5-bis[4,5-bis(methylthio)-1,3-dithiol-2-ylidene]-1,3,4,6-tetrathiapentalene).[9] This is probably related to the uniformly stacked crystal structures (vide infra). As shown in Fig. 1(b), the molecules of SMET-ST-TTP (**1a**) slip not only along the molecular long axis, but also along the molecular short axis: 6.25 and 1.95 Å for molecule A, 6.40 and 1.74 Å for molecule B. The interplanar distances A–A and B–B are 3.61 and 3.44 Å, respectively.

The donor molecules of SMET-ST-TTP (**1a**) stack uniformly along the *c* axis and form a θ-phase arrangement with the dihedral angle of 130° (Fig. 2(a)). In addition, the unit cell contains two molecular layers along the *b* axis (Fig. 2(b)). Although the charge-transfer salts of TMET-TTP universally form a θ-type structure, it is rather surprising that even the neutral molecule has the θ-phase structure, because the θ-type molecular arrangement is very rare in TTF-family neutral crystals. To our knowledge, the only known example is TTC_3-TTP.[10]

TMES-TS-TTP (1c): The molecular structure and the overlap mode of the neutral TMES-TS-TTP (**1c**) are shown in Figs. 3(a) and 3(b). The core π-skeleton is bent like an 'S' shape, where one methyl carbon extends out of the molecular plane and the other is located in the plane, as seen in the case of molecule B of the neutral SMET-ST-TTP (**1a**). The bent shape is similar to the neutral TTP molecule in TTC_3-TTP.[10]

The donor molecules of TMES-TS-TTP (**1c**) have a β-phase arrangement stacked uniformly along the *c* axis (Fig. 4(a)). The molecules of TMES-TS-TTP (**1c**) slip only along the molecular long axis (4.96 Å) (Fig. 3(b)). The distance between the molecular planes is 3.38 Å. The unit cell contains four molecular layers along the *b* axis (Fig. 4(b)), where the molecules are tilted in a manner of up-up-down-down.

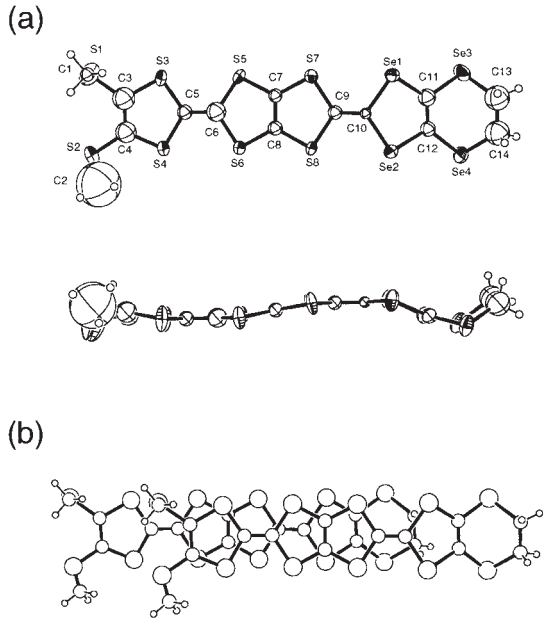

Fig. 3. ORTEP drawing (a) and overlap mode (b) of the neutral TMES-TS-TTP (**1c**).

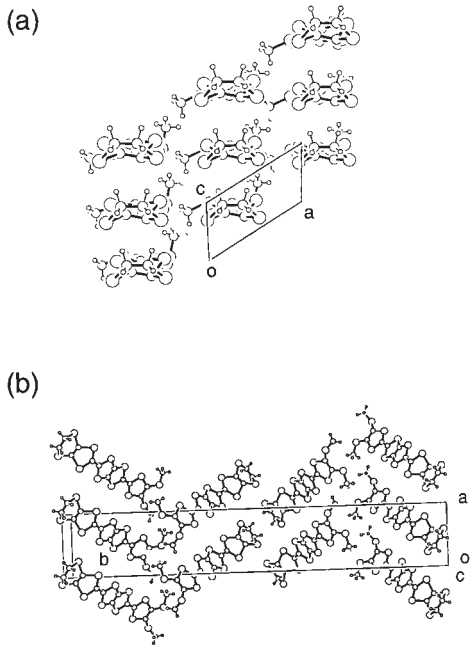

Fig. 4. Crystal structures of the neutral TMES-TS-TTP (**1c**). (a) View along the molecular long axis and (b) projection on the *ab* plane.

Table 3. Crystallographic Data of (SMET-ST-TTP: **1a**)$(AsF_6)_{0.32}$ and (SMES-BDS-TTP: **1d**)$(AsF_6)_{0.35}$ Together with (TMET-TTP)$(PF_6)_{0.27}$[a)]

	(SMET-ST-TTP: **1a**)$(AsF_6)_{0.32}$	(SMES-BDS-TTP: **1d**)$(AsF_6)_{0.35}$	(TMET-TTP)$(PF_6)_{0.27}$[b)]
Chemical formula	$C_{14}H_{10}As_{0.32}F_{1.92}S_8Se_4$	$C_{14}H_{10}As_{0.35}F_{2.10}S_4Se_8$	$C_{14}H_{10}F_{1.62}P_{0.27}S_{12}$
Formula weight	811.00	1004.27	600.88
Shape	Brown needle	Dark brown needle	Brown needle
Crystal system	Monoclinic	Monoclinic	Monoclinic
Space group	$P2_1/n$	$P2_1/n$	$P2_1/n$
a/Å	40.49(2)	41.02(2)	40.351(4)
b/Å	11.014(3)	11.268(5)	11.108(4)
c/Å	5.132(4)	5.176(5)	5.008(5)
α/°	90	90	90
β/°	93.45(5)	93.93(6)	93.50(5)
γ/°	90	90	90
V/Å^3	2284(2)	2387(2)	2240(2)
Z	4	4	4
D_{calc}/g cm^{-3}	2.457	2.837	
Temperature	r.t.	r.t.	r.t.
$R^{b)}/R_w^{c)}$	0.049/0.055	0.076/0.088	
Reflections used	1092 ($I > 3.0\sigma(I)$)	1071 ($I > 3.0\sigma(I)$)	

a) Ref. 2. b) $R = \Sigma||F_o| - |F_c||/\Sigma|F_o|$. c) $R_w = [\Sigma w(|F_o| - |F_c|)^2/\Sigma wF_o^2]^{1/2}$.

Crystal Structures of (SMET-ST-TTP: 1a)$(AsF_6)_{0.32}$ and (SMES-BDS-TTP: 1d)$(AsF_6)_{0.35}$. X-ray single crystal structure analyses of (SMET-ST-TTP: **1a**)$(AsF_6)_{0.32}$ and (SMES-BDS-TTP: **1d**)$(AsF_6)_{0.35}$ have been carried out. The crystallographic data are listed in Table 3. These salts are essentially isostructural to the θ-phase TMET-TTP salts.[2] The TMET-TTP salts are classified into two types; although the donor arrangements in the conducting sheets are entirely the same, the donor positions in the next conduction sheet are different. One is the PF_6 type ($P2_1/n$), and the other is the ReO_4 type ($P2_1/a$ when almost the same setting of the lattice constants with the PF_6 type, particularly β, is chosen).[2,5] The present salt belongs to the PF_6 type with the space group $P2_1/n$. All lattice constants of the Se salts increase with increasing the selenium contents. The ratio of the donor to the anion is determined to be almost 3:1 by the population analyses of the X-ray single crystal structure analyses. Moreover, the energy dispersion spectroscopy (EDS) from the ratio of S and As shows the DA_x composition to be $x = 0.37$ for SMET-ST-TTP (**1a**) and 0.33 for SMES-BDS-TTP (**1d**). Therefore, we can conclude an approximately 3:1 composition of both salts; this ratio is similar to that of the usual TMET-TTP salts, which have from 3:1 to 4:1 com-

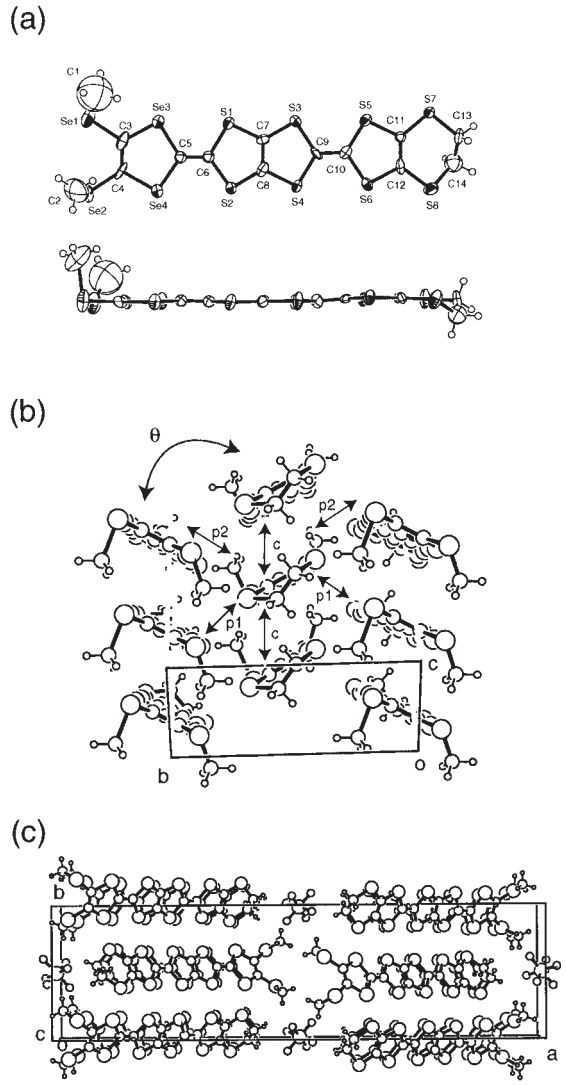

Fig. 5. Crystal structure of (SMET-ST-TTP: **1a**)$(AsF_6)_{0.32}$. (a) ORTEP drawing and atomic numbering of donors of (SMET-ST-TTP: **1a**)$(AsF_6)_{0.32}$. (b) Donor arrangement. (c) Projection onto the *ab* plane.

positions.

As shown in Fig. 5(a), the donors are almost planar, in contrast to the neutral molecules. One of the methylthio groups extends out of the molecular plane. The crystal structure is shown in Figs. 5(b) and 5(c). The donors make pseudo stacks along the *c* axis (Fig. 5(b)), in which the dihedral angle between the molecular planes of the adjacent stacks is 117° for both salts. This value is smaller than that of the usual TMET-TTP salts (128°), and is similar to 118° in (TMET-TS-TTP)$_2$(TCNQ).

Conducting Properties of (SMET-ST-TTP: 1a)$(AsF_6)_{0.32}$ and (SMES-BDS-TTP: 1d)$(AsF_6)_{0.35}$. The room temperature conductivity is 6 S cm^{-1} for (SMET-ST-TTP: **1a**)$(AsF_6)_{0.32}$ and 11 S cm^{-1} for (SMES-BDS-TTP: **1d**)$(AsF_6)_{0.35}$. As shown in Fig. 6, the temperature dependence of the resistivity shows a gradual increase down to 230 K for (SMET-ST-TTP: **1a**)$(AsF_6)_{0.32}$ and 180 K for (SMES-BDS-TTP: **1d**)$(AsF_6)_{0.35}$ and exhibits a steeper increase below these temperatures. This behavior is not better than that of the TMET-TTP salts, in which almost a flat resistivity is observed down to about 200 K.

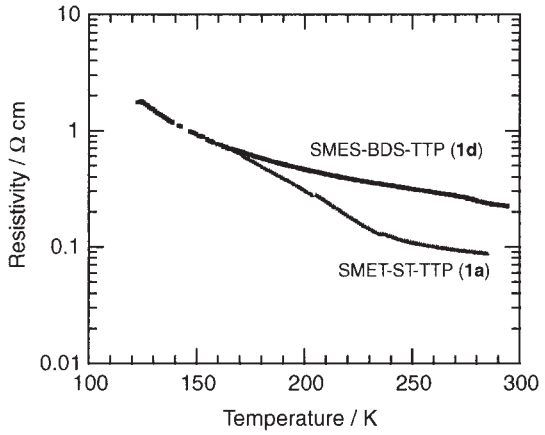

Fig. 6. Electrical resistivity of (SMET-ST-TTP: **1a**)-$(AsF_6)_{0.32}$ and (SMES-BDS-TTP: **1d**)$(AsF_6)_{0.35}$.

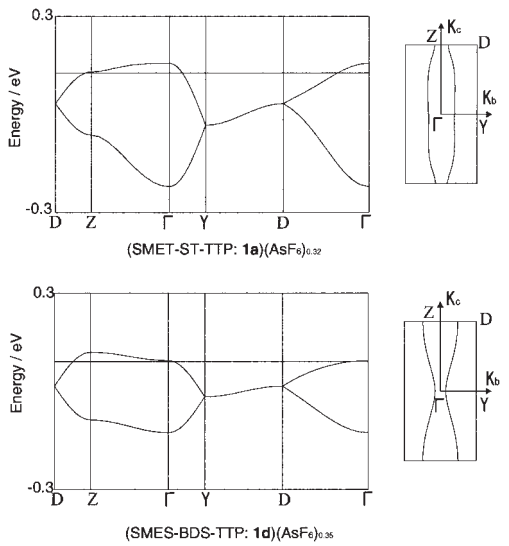

Fig. 7. Band structures and Fermi surfaces of (SMET-ST-TTP: **1a**)$(AsF_6)_{0.32}$ and (SMES-BDS-TTP: **1d**)$(AsF_6)_{0.35}$.

Table 4. The Intermolecular Overlap Integrals ($\times 10^{-3}$) of the Present Salts Together with (TMET-TS-TTP)$_2$(TCNQ)

	p1	p2	c
(SMET-ST-TTP: **1a**)$(AsF_6)_{0.32}$	−7.1	−2.3	1.7
(SMES-BDS-TTP: **1d**)$(AsF_6)_{0.35}$	−8.8	−0.3	1.3
(TMET-TS-TTP)$_2$(TCNQ)	5.1	3.2	4.9

Band Structures. The tight-binding band structures (Fig. 7) are calculated from the intermolecular overlap of HOMO (Table 4).[11] The selenium substitution does not much change the bandwidth, but the band structure is rather one-dimensional along the transverse (*b*) axis, and the resulting Fermi surface is open, in contrast to the usual θ-phase with the elliptic Fermi surface. This one-dimensionality comes from the exceedingly large p1 interaction compared with the p2 and c interactions (Table 4). The strong p1 interaction forms a zig-zag one-dimensional chain along the transverse (*b*) axis. Because a one-dimensional system is more susceptible to electron correlation than a two-dimensional system, this is the origin of the low conductivity.

Since the dihedral angle of the present salt (117°) is as small as 118° of (TMET-TS-TTP)$_2$(TCNQ), a similarly low metal–insulator transition temperature (∼120 K) is expected from the universal phase diagram of the θ-phase. Nonetheless, the conducting property is no more improved than that of the usual TMET-TTP salts ($T_{MI} \sim 200$ K). Se substitution reduces the Coulomb repulsion U, leading to stabilization of the metallic state. The actual shift is even opposite to this expectation. The electrochemical estimation of $U(E_2 - E_1)$, however, is not largely influenced by Se substitution (Table 1).

The unbalance of the intermolecular interactions is responsible for all of these discrepancies. The universal phase diagram of the θ-phase assumes an elliptical Fermi surface, even though the ground state is not metallic. The present compounds break this presupposition. One-dimensional system is more susceptible to electron correlation, and the insulating phase is stabilized. This is also related to the lower symmetry of the TTP θ-phase; the usual θ-phase has only one kind of diagonal interaction p, but the TTP θ-phase has p1 and p2.

Conclusion

Selenium substitution of the TMET-TTP molecule has been systematically carried out, where sulfur atoms of one or both of the outer 1,3-dithiole parts together with the methylthio or ethylenedithio sulfur atoms are substituted by selenium atoms. The crystal structure of the TMET-TTP family neutral crystal is revealed; SMET-ST-TTP (**1a**) forms a θ-type arrangement, even in the neutral crystal, whereas TMES-TS-TTP (**1c**) has a β-type structure. The charge-transfer salts, (SMET-ST-TTP: **1a**)$(AsF_6)_{0.32}$ and (SMES-BDS-TTP: **1d**)$(AsF_6)_{0.35}$, have a θ-phase arrangement of the donors with a relatively small dihedral angle of 117°. Although the small dihedral angle predicts a stable metallic state down to low temperatures, the actual conducting behavior is rather semiconductive. This discrepancy from the universal phase diagram is attributed to the unbalance of the overlap integrals induced by Se substitution. Other varieties of charge-transfer salts are under investigation.

Experimental

General Data. Trimethyl and triethyl phosphites were distilled under argon by fractional distillation. The melting points were determined with a Yanaco MP micro melting point apparatus. NMR spectra were obtained with a JEOL JNM-AL300 spectrometer. Cyclic voltamograms were measured on a Yanaco VMA-010 spectrometer. IR spectra were recorded on a SHIMADZU FTIR-8000 spectrometer.

2,3-Bis(2-cyanoethylthio)-6,7-bis(methylseleno)-1,4-dithia-5,8-diselenafulvalene (6). 4,5-Bis(methylseleno)-1,3-diselenol-2-one **4** (0.50 g, 10 mmol) and 4,5-bis(2-cyanoethylthio)-1,3-dithiole-2-thione **5** (1.14 g, 30 mmol) were heated in triethyl phosphite (15 mL) at 110 °C under nitrogen atmosphere for 2 h. After the triethyl phosphite was evaporated in vacuo, the residue was chromatographed on silica gel with CH_2Cl_2 as the eluent to afford **6** (0.64 g, 77%) as a red solid. Mp 121–122 °C; IR (KBr) ν_{max} 2925 (m), 2250 (m), 1418 (s), 889 (s), 709 (m) cm^{-1}; ^{1}H NMR (300 MHz, $CDCl_3$) δ 2.39 (s, 6H), 2.74 (t, 4H, $J = 7.2$ Hz), 3.08 (t, 4H, $J = 7.2$ Hz).

5-[4,5-Bis(methylseleno)-1,3-diselenol-2-ylidene]-1,3,4,6-tetrathiapentalene-2-thione (7). The dithiadiselenafulvalene **6** (0.64 g, 0.97 mmol) and NaOMe (0.63 g, 11.7 mmol) were reacted in acetone (5 mL) and methanol (4 mL) under nitrogen atmosphere for 40 min. Anhydrous zinc chloride (0.066 g, 0.49 mmol) in 3.0 mL methanol and tetrabutylammonium bromide (0.315 g, 0.97 mmol) in 3.0 mL methanol were successively added. The formed precipitates were collected by filtration, washed with methanol, and dried in vacuo. The residue was suspended in THF (12 mL), cooled to −80 °C, and acetic acid (1.4 mL) was added. The suspension was allowed to warm up to −20 °C over 3–4 h and then 1,1′-thiocarbonyldiimidazole (0.174 g, 0.97 mmol) in THF was added dropwise to the suspension, and the reaction mixture was allowed to warm up to room temperature. The solvent was removed by a rotary evaporator, and the residue was treated with methanol. The resulting precipitate was collected by filtration, washed with water and methanol, and dried in vacuo. The crude product was chromatographed on silica gel with CS_2 as an eluent to afford **7** (0.273 g, 48%) as a dark red solid. Mp 155–161 °C; IR (KBr) ν_{max} 1053 (s) cm^{-1} (C=S); ^{1}H NMR (300 MHz, $CDCl_3$) δ 2.37 (s, 6H).

SMET-ST-TTP (1a). The tetrathiapentalen-2-thione **2** (0.20 g, 0.5 mmol) and 4,5-bis(methylseleno)-1,3-diselenol-2-one **3** (0.40 g, 1.0 mmol) were reacted in 12 mL trimethyl phosphite and 15 mL toluene at 110 °C under nitrogen atmosphere for 2 h. The reaction mixture was cooled, and the resulting precipitate was collected by filtration, washed with hexane and methanol, and dried in vacuo. Chromatography (silica gel, CS_2) afforded orange solid of **1a** (42 mg, 12%). Mp 220–221 °C (dec); IR (KBr) ν_{max} 2917 (w), 2373 (w), 1414 (w), 1264 (w) cm^{-1}; ^{1}H NMR (300 MHz, $CDCl_3/CS_2 = 1/1$) δ 2.36 (s, 6H), 3.29 (s, 4H). Compounds **1b**–**1d** were prepared similarly.

TMET-ST-TTP (1b). 6% yield; brown solid; mp 230–231 °C (dec); IR (KBr) ν_{max} 2910 (w), 2372 (w), 1419 (w), 1285 (w) cm^{-1}; ^{1}H NMR (300 MHz, $CDCl_3/CS_2 = 1/1$) δ 2.42 (s, 6H), 3.28 (s, 4H).

TMES-TS-TTP (1c). 22% yield; brown solid; mp 238–239 °C (dec); IR (KBr) ν_{max} 2918 (w), 2373 (w), 1425 (w), 1262 (w) cm^{-1}; ^{1}H NMR (300 MHz, $CDCl_3/CS_2 = 1/1$) δ 2.40 (s, 6H), 3.36 (s, 4H).

SMES-BDS-TTP (1d). 14% yield; brown solid; mp 219–220 °C (dec); IR (KBr) ν_{max} 2917 (w), 2375 (w), 1406 (w), 1263 (w) cm^{-1}; ^{1}H NMR (300 MHz, $CDCl_3/CS_2 = 1/1$) δ 2.36 (s, 6H), 3.36 (s, 4H).

Electrochemical Crystal Growth. Brown needles of (SMET-ST-TTP: **1a**)$(AsF_6)_{0.32}$ and dark brown needles of (SMES-BDS-TTP: **1d**)$(AsF_6)_{0.35}$ were obtained on Pt electrodes by electrochemical oxidation; the donors (2 mg) and Bu_4NAsF_6 (50 mg) were dissolved in chlorobenzene (16 mL), and 0.2 μA current was applied for one week.

X-Ray Analysis. The data were collected on a Rigaku AFC7R diffractometer with graphite monochromated Mo Kα radiation and a rotating anode generator using the ω scan technique to a maximum 2θ of 60°. The structure was solved by the direct method (SIR 92) and refined by full-matrix least-squares analysis (anisotropic temperature factors for non-hydrogen atoms, except for isotropic factors for several atoms on account of the relatively poor crystal quality). All calculations ware performed using the teXsan crystallographic software package of Molecular Structure Corporation.

Crystallographic data have been deposited at the CCDC, 12 Union Road, Cambridge CB2 1EZ, UK and copies can be obtained on request, free of charge, by quoting the publication citation and the deposition numbers CCDC 216658–216661.

References

1 T. Mori, T. Kawamoto, Y. Misaki, K. Kawakami, H. Fujiwara, T. Yamabe, H. Mori, and S. Tanaka, *Mol. Cryst. Liq. Cryst.*, **284**, 271 (1996).

2 Y. Misaki, H. Nishikawa, T. Yamabe, T. Mori, H. Inokuchi, H. Mori, and S. Tanaka, *Chem. Lett.*, **1993**, 729; T. Mori, H. Inokuchi, Y. Misaki, H. Nishikawa, T. Yamabe, H. Mori, and S. Tanaka, *Chem. Lett.*, **1993**, 733.

3 H. Mori, S. Tanaka, and T. Mori, *Phys. Rev. B: Condens. Matter*, **57**, 12023 (1998).

4 T. Mori, Y. Misaki, H. Nishikawa, K. Kawakami, T. Yamabe, H. Mori, and S. Tanaka, *Synth. Met.*, **70**, 1179 (1995). Crystal data of (TMET-TTP)$_3$AsF$_6$: monoclinic, $P2_1/n$, $a = 40.12(4)$, $b = 11.068(8)$, $c = 4.994(5)$ Å, $\beta = 93.52(8)^\circ$, $V = 2229(3)$ Å^3.

5 M. Aragaki, H. Hoshino, T. Mori, Y. Misaki, K. Tanaka, H. Mori, and S. Tanaka, *Adv. Mater.*, **12**, 983 (2000).

6 F. Ogura and K. Takimiya, "Organoselenium Chemistry, A Practical Approach," ed by T. G. Back, Oxford University Press, New York (1999), p. 258.

7 K. Takimiya, A. Morikami, and T. Otsubo, *Synlett*, **1997**, 319; M. Kodani, K. Takimiya, Y. Aso, T. Otsubo, T. Nakayashiki, and Y. Misaki, *Synthesis*, **2001**, 1614; K. Takimiya, K. Yamane, Y. Aso, and T. Otsubo, *Mol. Cryst. Liq. Cryst.*, **379**, 65 (2002).

8 T. Mori, H. Inokuchi, Y. Misaki, T. Yamabe, H. Mori, and S. Tanaka, *Bull. Chem. Soc. Jpn.*, **67**, 661 (1994).

9 Y. Misaki, H. Nishikawa, K. Kawakami, S. Koyanagi, T. Yamabe, and M. Shiro, *Chem. Lett.*, **1992**, 2321.

10 S. Kimura, H. Kurai, and T. Mori, *Tetrahedron*, **58**, 1119 (2002).

11 T. Mori, A. Kobayashi, Y. Sasaki, H. Kobayashi, G. Saito, and H. Inokuchi, *Bull. Chem. Soc. Jpn.*, **57**, 627 (1984).